JOURNAL OF GEOPHYSICAL RESEARCH, VOL. ???, XXXX, DOI:10.1029/,

The location of the Earth's magnetopause: a comparison of modeled position and in-situ Cluster data

N. A. Case[1] and J. A. Wild[1]

Space Plasma Environment and Radio Science Group, Department of Physics, Lancaster University, Lancaster, LA1 4YB, UK (n.case@lancaster.ac.uk)

[1]Department of Physics, Lancaster University, Lancaster, UK.

Abstract. Exploiting eight years of magnetic field data from the Cluster mission, we employ an automated magnetopause crossing detection routine to determine the magnetopause location over varying magnetic latitude and local time. For a period spanning nearly one solar cycle we build a database of 2709 magnetopause crossings and compare these locations to the magnetopause models of *Petrinec and Russell* [1996], *Shue et al.* [1998], *Dmitriev and Suvorova* [2000] and *Lin et al.* [2010]. We compare our detected locations with the predicted locations for a variety of solar wind conditions and positions on the magnetopause. We find that, on average, the *Petrinec and Russell* [1996] and *Shue et al.* [1998] models overestimate the radial distance to the magnetopause by $\sim$1 R_E (9%) whilst the *Dmitriev and Suvorova* [2000] and *Lin et al.* [2010] models underestimates it by 0.5 R_E (4.5%) and 0.25 R_E (2.3%) respectively. Some varying degree of control on the differences between the predicted and encountered locations, by the solar wind and location parameters, are found.

1. Introduction

The accurate determination of the size and configuration of the magnetosphere is acutely important when investigating interactions between the interplanetary and near-Earth space environments. Understanding how the solar wind and interplanetary magnetic field (IMF) constrains the Earth's magnetosphere requires accurate specification of the magnetopause location under a variety of conditions.

Chapman and Ferraro [1931] first introduced the concept of a magnetopause whose shape and size is dependent upon the solar wind dynamic pressure (P_d). Since then, several empirical models have been developed to describe the shape and location of the magnetopause based on *in situ* satellite measurements. Examples include *Fairfield* [1971], *Roelof and Sibeck* [1993], *Petrinec and Russell* [1996], *Shue et al.* [1997] and *Suvorova et al.* [1999]. The accuracy of such models can be assessed further by comparing the predicted magnetopause position with spacecraft observations of the boundary not included in the original modelling process (e.g. *Shue et al.* [1998], *Šafránková et al.* [2002] and *Dmitriev et al.* [2011]).

Although it is possible to survey the magnetopause location via changes in the observed magnetic field and plasma characteristics at a spacecraft, the boundary can vary in thickness from around 400-700 km [*Berchem and Russell*, 1982] and, depending upon a spacecraft's trajectory, it may pass through the boundary rapidly (∼seconds) or skim along the magnetopause passing in and out in multiple times in quick succession over a longer period (∼hours).

Manual determination of a magnetopause crossing can be a labor-intensive task requiring the identification of discontinuities in magnetic field data, plasma data or both. In a large scale survey, with hundreds or thousands of potential crossings, this can become impractical and an effective automated routine is desirable. Such an automated method would need to exploit a clearly-defined set of criteria to determine what physical parameter changes constitute a boundary crossing event over an appropriate spatial and temporal timescale.

In this study, a modified version of the *Ivchenko et al.* [2000] automated magnetopause crossing routine is applied to ∼8 years of magnetic field data from the Cluster mission to determine the location of the magnetopause. The detected crossings locations are then compared to the commonly-used magnetopause models of *Petrinec and Russell* [1996], *Shue et al.* [1998], *Dmitriev and Suvorova* [2000] and *Lin et al.* [2010].

Petrinec and Russell [1996] presents a cylindrically symmetrical empirical magnetopause model based on data from the ISEE satellite missions [*Song et al.*, 1988] and is an amalgamation of two earlier models: *Petrinec et al.* [1991] and *Petrinec and Russell* [1993]. *Petrinec et al.* [1991] modeled the dayside magnetopause using a best fit ellipsoid function to ISEE 1 and 2 magnetopause crossings; *Petrinec and Russell* [1993] used magnetic pressure balancing of the magnetopause to infer the location of the magnetotail. *Petrinec and Russell* [1996] then combine these two models with a smooth connection at the terminator.

The *Petrinec and Russell* [1996] model ignores nonaxisymmetric functions on the dayside magnetopause (including the magnetic cusp regions). It has a range of validity for the input parameters of -10 $< B_z <$ 10 nT and 0.5 $< P_d <$ 8 nPa and has different modeling parameter values based upon the orientation of B_z.

The *Shue et al.* [1998] model is an improved version of the earlier *Shue et al.* [1997] model which was derived as an empirical best fit to data from several magnetospheric satellites, including ISEE 1 & 2 and IMP 8. After further testing with a magnetic cloud event in 1997, in which the magnetopause passed inside geosynchronous orbit, *Shue et al.* [1998] improved the functional forms of the *Shue et al.* [1997] model to better represent the effect of P_d on the flaring angle and of B_z on the subsolar standoff distance. As with *Petrinec and Russell* [1996], the *Shue et al.* [1998] model is cylindrically symmetric and does not account for the magnetospheric cusp regions.

The previous two models are both 2-dimensional and empirically derived using two input parameters: the magnetic field component B_z and the solar wind dynamic pressure (P_d) as these two parameters have been found to be significant in modeling the magnetopause location by many previous studies (e.g. *Petrinec et al.* [1991], *Sibeck et al.* [1991] and *Roelof and Sibeck* [1993]). *Dmitriev and Suvorova* [2000], however, used an Artificial Neural Network (ANN) to develop a complex, multi-parameter, 3-D model of the magnetopause.

Dmitriev and Suvorova [2000] employ the selection criteria developed by Kuznetsov and Suvorova [1997] on dayside magnetopause crossings from *Roelof and Sibeck* [1993] and geosynchronous crossings from Kuznetsov and Suvorova [1997] to build a data set of 999 magnetopause crossings (assuming a mirrored symmetry in the ecliptic plane) to input into the ANN model. Initially, 30 different parameters were included in the model, however, *Dmitriev and Suvorova* [2000] were able to reduce the number of required inputs to five parameters (λ - the GSE latitude , φ - the GSE longitude, B_y (GSM), B_z (GSM) and $\ln[P_d]$) whilst keeping a model correlation accuracy of 0.92 and a standard deviation of

1.04 R_E [*Dmitriev and Suvorova*, 2000]. The [*Dmitriev and Suvorova*, 2000] is asymmetric in the dawn-dusk plane.

With the ANN model there are several validity ranges on the input parameters, which *Dmitriev and Suvorova* [2000] state should keep the relative error under 10%. The longitude and latitude (GSE) should be between ± 90 degrees and ± 80 degrees respectively. The magnetic field components should be between: -20 $< B_y <$ 20 nT and -20 $< B_z <$ 20 nT and the dynamic pressure should be between 0.5 $< P_d <$ 40 nPa.

Lin et al. [2010] present a three-dimensional asymmetric magnetopause model which is built upon the *Shue et al.* [1997] magnetopause model. In addition to exploiting the solar wind dynamic pressure and the B_z component of the IMF as model parameters, the *Lin et al.* [2010] model also takes into account the solar wind magnetic pressure (P_m) and the Earth's magnetic dipole tilt angle (ϕ).

The *Lin et al.* [2010] model was developed using 980 magnetopause crossings from a range of satellite missions (including Geotail, IMP and Cluster) with 5 minute averaged solar wind parameters and 1482 Hawkeye magnetopause crossings with hourly solar wind parameters. Using the Levenberg-Marquardt method for non-linear multi-parameter fitting, *Lin et al.* [2010] determine the important control parameters for the magnetopause size and shape and the relationships between them.

Unlike most magnetopause models, including *Petrinec and Russell* [1996] and *Shue et al.* [1998], the *Lin et al.* [2010] model is able to account for the north-south asymmetry of the magnetopause and for the indentations near the magnetic cusps and so should provide more accurate results in these regions.

In the sections that follow, we discuss how we utilize the *in situ* magnetic field data and how we modify the *Ivchenko et al.* [2000] magnetopause crossing detection routine to determine the location of the magnetopause for eight years of satellite data. We then compare our results to the models previously described.

2. In situ magnetic field data

The four European Space Agency (ESA) Cluster spacecraft have been in an elliptical polar orbit around the Earth since 2000. During the northern hemisphere's winter months the spacecraft pass through the dayside magnetopause on their outward trajectory from perigee to apogee. Over the mission lifetime, the orbital configuration has varied resulting in encounters with the magnetopause over a wide range of latitudes and at varying local times, due to the Earth's orbit about the Sun. The wide range of latitudes accessible to Cluster is in contrast to some earlier studies (e.g. *Ivchenko et al.* [2000] and *Dušík et al.* [2010]) that focussed on spacecraft measurements at low latitudes.

The magnetic field data are collected by each spacecraft's FGM instrument which consists of two three-axis fluxgate magnetometers [*Gloag et al.*, 2010]. The FGM data used in this study are obtained from the Cluster Active Archive (see *Laakso et al.* [2010]) at four second resolution and are presented in this paper in the GSM co-ordinate system. Magnetic field data are used exclusively, rather than in combination with plasma data, as they are one of the most commonly available spacecraft data sets (both for Cluster and other missions).

Solar wind data, which are required as an input into the models, are obtained from the OMNIweb service (http://omniweb.gsfc.nasa.gov) at one minute resolution and are then averaged to five minute resolution, as in *Shue et al.* [1997]. This"High Resolution OMNI"

data set contains an interspersal of ACE, Wind, IMP 8 and Geotail data which have been time-shifted to the bow shock nose. The solar wind data are averaged to five minute resolution since it is unclear how quickly the magnetopause responds to changing solar wind conditions and the averaging also removes any ambiguity due to the lagging process. Additionally, propagation times across the magnetosheath are ∼4 mins (e.g. Khan and Cowley [1999] and *Wild et al.* [2009]) and so this averaged data is generally representative of the conditions at the magnetopause.

3. Methodology

We base our magnetopause crossing selection criteria on those of *Ivchenko et al.* [2000], whose detection routine was applied to two and a half years of three-second resolution magnetic field data from the Geotail mission. The four *Ivchenko et al.* [2000] criteria for the determination of a crossing are:

1. the transition across the magnetopause should be completed within 30s;

2. the standard deviation of the magnetospheric magnetic field is required to be less than 40% of the magnetic field on the magnetosheath side of the assumed boundary;

3. the northward component of the magnetospheric magnetic field is required to exceed 10 nT and;

4. the northward component of the magnetospheric magnetic field is required to be at least a factor of 1.3 times greater than the corresponding magnetosheath component.

Since Geotail only encountered the magnetopause in a narrow range of latitudes, around $\pm 2R_E$ from the GSM-x axis (typically in a skimming-type configuration) [*Nishida*, 1994], whereas Cluster passes through the magnetopause at a range of latitudes, the *Ivchenko et al.* [2000] criteria require modification. Specifically, *Ivchenko et al.* [2000] consider the difference in the northward component of the magnetic field (B_z) either side of the magnetopause boundary. This generally works well except in the following two cases: (1) when the IMF is primarily orientated northward, in which case the B_z component of the magnetic field is similar in both the magnetosheath and magnetosphere, and (2) at high latitudes, where B_z tends to zero as the magnetic field is directed primarily toward/away from the Earth (in the cusp region this changes with B_z once again becoming dominant but now in the opposite direction). Case (1) is somewhat difficult to account for, but to account for case (2): at high latitudes (where the angle between the spacecraft position in the GSM x-y plane is greater than 45 degrees) we instead use the radial component of the magnetic field (B_r).

Data from all four Cluster spacecraft between 2002-2010 are analyzed and, using the modified *Ivchenko et al.* [2000] criteria, magnetopause crossings are detected. To reduce data processing time, we focus on time intervals centered on the predicted magnetopause crossings as given in the Cluster predicted events catalog [*Hapgood et al.*, 1997]. In order to avoid a bias toward finding the magnetopause in close proximity to where the Cluster planning software (which employs the *Sibeck et al.* [1991] magnetopause model) predicts it will be located, we examine data from a four hour window. Over this window, the spacecraft typically travel a distance of $\sim 5R_E$. We thus expect to capture virtually all potential magnetopause crossings.

For determination of a magnetopause crossing, we employ a running average method on the four hour window of magnetic field data. Two three minute segments of magnetic field data, separated by a 32 second gap, are selected and tested against the following modified *Ivchenko et al.* [2000] crossing criteria. If a crossing is not encountered then the two segments of data chosen are shifted along in time by four seconds, however, if a crossing is encountered then the segments chosen are shifted forward by 10 minutes. All criteria must be met for a crossing to be determined.

1. The transition across the magnetopause boundary should be completed within 32 seconds (equivalent to eight spins of the Cluster spacecraft). The time of the crossing event is recorded as when the spacecraft first crosses into the boundary layer and so by enforcing this transition time limit we ensure that the recorded time of crossing is accurate.

2. Multiple magnetopause crossings should not occur within 10 minutes. Multiple crossings may occur when the spacecraft is skimming the magnetopause or when the magnetopause location is rapidly fluctuating; rather than having multiple crossing events, we instead choose the first event to represent the crossing location.

3. The standard deviation of the three minute window of magnetosheath magnetic field must be greater than 4.5 on average and it must be a factor of 2.5 times larger than the standard deviation of the three minute window of magnetospheric magnetic field. This criteria requires that the magnetic field observed in the magnetosheath is fluctuating by a larger amount than the magnetospheric magnetic field.

4. At low latitudes the B_z, and at high latitudes the B_r, component of the magnetospheric magnetic field must be greater than 10nT, since we take this to be a conservative estimate of the minimum terrestrial magnetosphere field strength.

5. The particular magnetospheric magnetic field component, as determined by criteria (4), must be a factor of at least 1.3 times greater the corresponding magnetosheath magnetic field component. Although this may rule out occasions where the orientation of the IMF is similar of that to the magnetosphere, this factor was determined to be most appropriate in preventing small changes in the magnetic field from registering as crossing events.

An example of a magnetopause encounter is shown in Figure 1. The three panels on the left of the figure present magnetic field data from Cluster 1 showing the overall magnetic field strength $|B|$, the appropriate magnetic field component (in this case B_r), the three minute running standard deviation of $|B|$, and the clock angle of the measured magnetic field, respectively. The clock angle is defined as the arctangent of the y-component of the magnetic field over the z-component and is shown as measured at Cluster (yellow) and the equivalent parameter predicted at the bowshock by OMNIweb (blue). The dashed vertical black line in the left panel indicates the time at which the Cluster predicted events catalog suggested a crossing would occur; the dashed red line indicates the time at which the automated routine detected a crossing. The panel on the right of the figure shows the Cluster spacecraft's position and a Tsyganenko-96 magnetic field model magnetosphere in GSE co-ordinates. The modeled magnetosphere is determined for the time of the detected crossing and is projected into the GSE X-Z plane (i.e. at $\mathrm{Y}_{GSE} = 0$).

4. Results and Discussion

In total, 2709 crossings were detected using the automated routine described above, reducing to 2640 useful crossings due to missing/bad data in the OMNIweb database. This value is significantly less than 7418 predicted crossings listed in the predicted events catalog, however, this was to be expected since our selection criteria are somewhat conservative.

The locations of these crossings are shown in Figure 2. The four panels in Figure 2 represent different co-ordinate planes (from top left to bottom right): the noon-midnight meridian of the magnetosphere (with the Sun off to the left-hand side of the plot), a projection of the GSM equatorial plane from above the magnetic North Pole, a view of the Earth from the direction of the Sun and a projection of the radial distance to the magnetopause from the Earth as a function of X_{GSM} position.

Cluster's encounters with the magnetopause were detected over almost a full 180 ° range of latitudes with particularly high density regions at $\pm$ 10 R_E in the z-axis and over local times of 0900-1500 due to Cluster's orbital configuration.

The detected crossing locations were compared with the predicted magnetopause locations for each of the four models discussed in the Introduction. The steps involved in calculating the radial separation distance (Δr) between the spacecraft location and the modeled magnetopause location are as follows. Firstly, we define the separation distance as the radial location of the spacecraft subtracted from the radial location of the magnetopause:

$$\Delta r = r_{mp} - r_{sc} \tag{1}$$

where r_{sc}, the radial distance to the spacecraft, is defined as the length of the vector drawn from the Earth to the spacecraft location in the x-ρ plane:

$$r_{sc} = \sqrt{{x_{sc}}^2 + \rho^2} \tag{2}$$

where ρ is the length of the spacecraft position vector in the y-z plane:

$$\rho = \sqrt{{y_{sc}}^2 + {z_{sc}}^2} \tag{3}$$

and where r_{mp} is the radial distance to the modeled magnetopause, as determined individually for each model at spacecraft angle θ, the latitude in the x-ρ plane:

$$\theta = \arctan\left(\frac{\rho}{x_{sc}}\right) \tag{4}$$

where x_{sc}, y_{sc} and z_{sc} are the spacecraft's location in GSM x, y and z components.

Due to the validity limitations on the input parameters of the models we were able to compare 2599 crossings to the *Petrinec and Russell* [1996] model and 2621 crossings to the *Dmitriev and Suvorova* [2000] model. All 2640 crossings were compared against the *Shue et al.* [1998] and *Lin et al.* [2010] models since no parameter restrictions were specified.

Figure 3 compares the location of the *Petrinec and Russell* [1996] model magnetopause to the crossings detected by Cluster using the technique described above. The median difference in the radial location is found to be 1.06 R_E, with the positive value indicating that the modelled magnetopause location is typically radially further from the Earth than the detected location. The histogram is generally symmetrically distributed about the median.

Figure 4 is a comparison between the *Shue et al.* [1998] model and our detected crossings. We find that the median difference is 1.48 R_E, again indicating that the median modeled location was radially further out from the Earth than the detected location. The histogram

is symmetrical around the median, though with a greater spread than with the *Petrinec and Russell* [1996] model.

The detected crossing locations and the *Dmitriev and Suvorova* [2000] modeled magnetopause locations are compared in Figure 5. The median difference between the model and the detected crossing locations is -0.52 R_E, which, opposite to the previous two models, shows that the median modeled location was radially closer to the Earth than the detected crossing location. The difference distribution is non-symmetrical with a substantial tail, of approximately 250 (10%) events, at radial differences less than -3 R_E.

In Figure 6 the detected and predicted crossing locations are compared for the *Lin et al.* [2010] model. The median difference is -0.24 R_E which, as with the *Dmitriev and Suvorova* [2000] model, suggests that, in general, the *Lin et al.* [2010] model slightly underestimates the distance to the magnetopause. The distribution of differences is similar to the *Dmitriev and Suvorova* [2000] distribution but with a smaller tail region (approximately 5% of events). Over half of the data lie within $\pm 1 R_E$.

The radial differences between the detected crossing locations and the four models are shown for four parameters (clock angle, B_z, P_d and θ) in Figure 7. The number of crossings are represented by the color-scaled density bins. The crosses indicate the median value for the row of bins and the error bars represent the standard deviation of the distribution in each row.

The clock angle has little or no influence on the radial difference for any of the models. There is little apparent relationship between the radial differences of the modeled and observed magnetopause locations and B_z for the *Petrinec and Russell* [1996] model. At B_z<4nT, the radial differences for the *Shue et al.* [1998] model decrease from around 2 R_E

to around 0 R_E. The *Dmitriev and Suvorova* [2000] and *Lin et al.* [2010] model plots have a similar form as the *Shue et al.* [1998] plot but are off-set by about -2 R_E. Approximately 11% of the data fall below a B_z value of less than -4nT.

With the P_d parameter, there is some small dependence of the radial difference for the *Petrinec and Russell* [1996] model. At larger P_d, the radial differences for the *Petrinec and Russell* [1996] model increase, however, the opposite is true for the other three models. As P_d increases, the radial differences decrease for the *Shue et al.* [1998] model and become increasingly negative for the *Dmitriev and Suvorova* [2000] and *Lin et al.* [2010] models.

The spacecraft angle, θ, has a small influence on the radial difference, with increasing radial differences at increasing spacecraft angles (i.e. at high latitudes), for both the *Petrinec and Russell* [1996] and *Shue et al.* [1998] models. A more pronounced, but opposite, effect is noticed with the *Dmitriev and Suvorova* [2000] model where increasing spacecraft angle results in an increasingly negative radial difference. The radial differences for the *Lin et al.* [2010] model do not seem to be affected by the spacecraft angle.

The primary aim of this study was to as to use an automated routine, rather than manual inspection, to determine crossing events and then compare these events to the magnetopause models. However, to ensure that the results presented are statistically valid, and not the product of an erroneous automated routine, we conducted a sample study on the results. A random sample totalling 20% of the data was manually analyzed and any false crossing identification events were removed. Of the 528 random events, 341 were identified as accurate crossing events. These were then plotted and compared to the main plots and we found similar distributions for all; see Figure 8 for the comparison of the medians from the full population and from the sample.

297 On inspection of those events where the routine had identified a crossing yet no such
298 crossing had occurred, we found that most events had only just qualified under our cri-
299 teria. Increasing the magnitude of the discontinuity in the magnetic field data required
300 to determine a crossing would help eliminate these false positives further but would also
301 severely impact the total number of accurate magnetopause crossing detections.

5. Summary

302 In this investigation, we created a more generalized version of the *Ivchenko et al.* [2000]
303 magnetopause crossing detection routine to explore its application at higher latitudes.
304 After applying our modified criteria to 8 years of Cluster magnetic field data we have
305 identified 2709 crossings of which we were able to compare 2640 crossings to four models:
306 two commonly used 2-D empirical models, one 3-D ANN model and one asymmetric
307 empirical 3-D model.

308 We find that the two empirical 2-D models, *Petrinec and Russell* [1996] and *Shue*
309 *et al.* [1998], generally agree well with each other. They both produce similar median
310 differences and interquartile ranges, when compared to our detected crossing locations,
311 though this is perhaps not unexpected since when *Shue et al.* [1998] compared their model
312 with that of *Petrinec and Russell* [1996] they found that the two models generally correctly
313 predicted dayside magnetopause crossings (the major differences occurring in the flanks).
314 Additionally, both models were developed using very similar datasets and so one might
315 expect similar results when using these models.

316 The radial differences between the detected crossing locations and the *Petrinec and*
317 *Russell* [1996] and *Shue et al.* [1998] modeled locations are off-set about a median of just
318 over 1 R_E. This indicates that, in general, the models over-estimate the radial distance

to the magnetopause (by about 9%). There are a couple of reasons for why this may be the case. Firstly, the vast majority of the data in their crossing databases were obtained using near-equatorial satellite missions (ISEE-1 & 2). It is now well known that, under the same external conditions, the magnetopause is greater in size in the equatorial plane than in the meridional plane [*Dmitriev and Suvorova*, 2000]. Since these two models were based on low-latitude satellite missions, at middle latitudes where the magnetopause is flatter, they would tend to overestimate the distance to the magnetopause.

This assumption is strengthened when the differences between the modeled magnetopause locations of *Petrinec and Russell* [1996] and *Shue et al.* [1998] and the detected locations are compared with the spacecraft angle. The models agreed well with the detected locations at spacecraft angles (θ) of $< 40^{\circ}$ but there was an increase in the difference at angles larger than this.

Secondly, the majority of the ISEE 1 & 2 data was collected during a period of of rising solar activity (1977-1979) which resulted in an increased frequency of co-rotating high-speed solar wind streams. The trailing edges of such solar wind streams are often accompanied by regions of quasi-radial IMF and it has been shown that, in such conditions, the magnetopause is expanded beyond its normal location [*Suvorova et al.*, 2010]. Hence, in the case of *Petrinec and Russell* [1996] and *Shue et al.* [1998], who used large amounts of data from this period to build their models, we should expect that the models will overestimate the distance to the magnetopause during normal IMF conditions.

There was a clear trend in the radial difference between the detected location and the modeled locations of *Shue et al.* [1998], *Dmitriev and Suvorova* [2000] and *Lin et al.* [2010] when compared with solar wind dynamic pressure. For *Shue et al.* [1998], the differences

range from a median of 2 R_E at $P_d < 1$ nPa through to -2 R_E at $P_d = 8$ nPa, with 0 R_E occurring at around 4 nPa. The results of this plot closely match those of *Dušík et al.* [2010] who compared 6649 THEMIS magnetopause crossings to the *Shue et al.* [1998] model, though we compare crossings over a much wider range of latitudes. For *Dmitriev and Suvorova* [2000] and *Lin et al.* [2010], there was similar trend to *Shue et al.* [1998] but the data was distributed approximately -2 R_E from the *Shue et al.* [1998] distribution.

The median difference between the predicted and measured location of the magnetopause for the *Dmitriev and Suvorova* [2000] and *Lin et al.* [2010] models both suggest that the models underestimate the radial distance to the magnetopause by 0.52 R_E and 0.24 R_E respectively whereas the other two models overestimate it: by 1.06 R_E for *Petrinec and Russell* [1996] and by 1.48 R_E for *Shue et al.* [1998].

As with many automated routines, we acknowledge that the modified *Ivchenko et al.* [2000] routine used in this study will not identify all crossings and that it may determine a crossing when no such event occurred. It does, however, provide a statistically valid approach to detecting crossings with a large-scale data set.

The *Ivchenko et al.* [2000] crossing criteria, and our modified version of them, are based purely on magnetic field data. Whilst this is convenient, since magnetic field data is the most commonly available, straightforward and reliable data set, it is well known that there are clear differences in the plasma characteristics between the magnetosheath and magnetosphere regimes. Indeed, some studies (e.g. *Hapgood and Bryant* [1990]) primarily use the plasma characteristics as the defining data set for determination of magnetopause crossings. Incorporation of plasma data criteria into the modified *Ivchenko et al.* [2000] crossing criteria requires further investigation.

In addition, we have used magnetic field data from the Cluster mission to determine the magnetopause location since the spacecraft encountered the magnetopause at varying magnetic latitude and local time. This was an improvement on other magnetopause studies, whose spacecraft often visited similar regions of space. Nevertheless combining data from multiple spacecraft missions, to increase spatial and temporal coverage, may prove to be a useful future exercise.

Acknowledgments. We gratefully acknowledge the NASA/GSFC Space Physics Data Facility's OMNIWeb service. We also acknowledge the Cluster Active Archive data facility and the Cluster FGM team for the use of the Cluster data. NAC is supported by an STFC studentship.

References

Berchem, J., and C. T. Russell (1982), The Thickness of the Magnetopause Current Layer: ISEE 1 and 2 Observations, *J. Geophys. Res., 87,* A4, 2108–2114.

Chapman, S., and V. C. A. Ferraro (1931), A new theory of magnetic storm, I, The initial phase, *J. Geophys. Res., 36*, 77

Dmitriev, A. V., and A. V. Suvorova (2000), Three-dimensional artificial neural network model of the dayside magnetopause, *J. Geophys. Res., 105*(A8), 18909–18918, doi:10.1029/2000JA900008.

Dmitriev, A. V., Suvorova, A. V., J.-K. Chao (2011), A predictive model of geosynchronous magnetopause crossings, *J. Geophys. Res.*, *116*, A05208, doi:10.1029/2010JA016208

Dušík, Š., G. Granko, J. Šafránková, Z. Němeček and K. Jelínek (2010), IMF cone angle control of the magnetopause location: Statistical study, *Geophys. Res. Lett, 37*, L19103, doi:10.1029/2010GL044965.

Fairfield, D. H. (1971), Average and unusual locations of the Earth's magnetopause and bow shock, *J. Geophys. Res., 78*, 23, 6700–6716

Gloag, J. M., E. A. Lucek, L.-N. Alconcel, A. Balogh, P. Brown, C. M. Carr, C. N. Dunford, T. Oddy and J. Soucek (2010), FGM Data Products in the CAA, in *The Cluster Active Archive*, edited by H. Laakso, M. Taylor and C. Escoubet, Astrophysics and Space Science Proceedings, 109–128, Springer Netherlands, doi:10.1007/978-90-481-3499-1_7

Hapgood, M. A., T. G. Dimbylow, D. C. Sutcliffe, P. A. Chaizy, P. S. Ferron, P. M. Hill and X. Y. Tiratay (1997), The Joint Science Operations Centre, *Space Sci. Rev.*, *79*, 487–525

Hapgood, M. A., and D. A. Bryant (1990), Re-ordered electron data in the low-latitude boundary layer, *Geophys. Res. Lett, 17*, 2043–2046

Ivchenko, N. V., D. G. Sibeck, K. Takahashi and S. Kokubun (2000), A statistical study of the magnetosphere boundary crossings by the Geotail satellite, *Geophys. Res. Lett, 27*, 18, 2881–2884

Khan, H. and S. W. H. Cowley (1999), Observations of the response time of high-latitude ionospheric convection to variations in the interplanetary magnetic field using EISCAT and IMP-8 data, *Ann. Geophys.*, *17*, 1306–1335

Kuznetsov, S. N., and A. V. Suvorova (1997), Magnetopause shape near geosynchronous orbit (in Russian), *Geomagn. Aeron, 37*(3), 1–11

Laakso, H., M. Taylor and C. P. Escoubet (Eds.) (2010), *The Cluster Active Archive*, Astrophysics and Space Science Proceedings, Springer New York

Lin, R. L., X. X. Zhang, S. Q. Liu, Y. L. Wang, and J. C. Gong (2010), A three-dimensional asymmetric magnetopause model, *J. Geophys. Res.*, *115*, doi:10.1029/2009JA014235

Nishida, A. (1994), The GEOTAIL Mission, *Geophys. Res. Lett, 21*, 25, 2871–2873, doi:10.1029/94GL01223

Petrinec, S. M., and C. T. Russell (1993), An empirical model of the size and shape of the near-Earth magnetotail, *Geophys. Res. Lett, 20*, 2695

Petrinec, S. M., and C. T. Russell (1996), Near-Earth magnetotail shape and size as determined from the magnetopause flaring angle, *J. Geophys. Res., 101*(A1), 137–152

Petrinec, S. M., P. Song, and C. T. Russell (1991), Solar cycle variation in the size and shape of the magnetopause, *J. Geophys. Res., 96*, 78936-7896

Roelof, E. C. and D. G. Sibeck (1993), Magnetopause shape as a bivariate function of interplanetary magnetic field B_z and solar wind dynamic pressure, *J. Geophys. Res., 98*, 21421-21450, doi:10.1029/93JA02362

Šafránková, J., Z. Němeček, Š. Dušík, L. Přech, D. G. Sibeck, and N. N. Borodkova (2002), The magnetopause shape and location: a comparison of the Interball and Geotail observations with models, *Ann. Geophys.*, *20*, 301–309

Shue, J. H., J. K. Chao, H. C. Fu, C. T. Russell, P. Song, K. K. Khurana and H. J. Singer (1997), A new functional form to study the solar wind control of the magnetopause size and shape, *J. Geophys. Res., 102*, 9497–9511

Shue, J.-H., P. Song, C. T. Russell, J. T. Steinberg, J. K. Chao, G. Zastenker, O. L. Vaisberg, S. Kokubun, H. J. Singer, T. R. Detman and H. Kawano (1998), Magnetopause

location under extreme solar wind conditions, *J. Geophys. Res., 103*(A8), 17691–17700, doi:10.1029/98JA01103

Sibeck, D. G., R. E. Lopez, and E. C. Roelof (1991), Solar wind control of the magnetopause shape, location, and motion, *J. Geophys. Res.*, *96(A4)*, 5489-5495, doi:10.1029/90JA02464

Song, P., R. C. Elphic and C. T. Russell (1988), ISEE 1 and 2 observations of the oscillating magnetopause, *Geophys. Res. Lett, 15*, 744

Suvorova A.V, A.V. Dmitriev, S.N. Kuznetsov (1999), Dayside magnetopause models, *Rad. Meas.*, *30*(5), 687–692.

Suvorova, A. V., J.-H. Shue, A. V. Dmitriev, D. Sibeck, J. McFadden, H. Hasegawa, K. Ackerson, K. Jelinek, J. Safrankova, Z. Nemecek (2010), Magnetopause expansions for quasi-radial interplanetary magnetic field: THEMIS and Geotail observations, *J. Geophys. Res.*, *115*, A10216, doi:10.1029/2010JA015404.

Wild, J. A., E. E. Woodfield and S. K. Morley (2009), On the triggering of auroral substorms by northward turnings of the interplanetary magnetic field, *Ann. Geophys.*, *27*(9), 3559–3570, doi:10.5194/angeo-27-3559-2009

Figure 1. An example of the plots produced by the crossing detection routine. The three panels on the left of the figure present the magnetic field data (the magnetic field strength $|B|$ (black) and chosen magnetic field component which is B_r in this case (purple), the running standard deviation of a three minute segment of the magnetic field strength, and the clock angle (measured with Cluster in blue and predicted by OMNIweb in yellow). The red dashed line indicates a detected inward crossing; the black dashed line indicates the time the spacecraft were predicted to cross the magnetopause. The panel on the right shows the spacecraft position and a modeled magnetosphere for the time of the crossing (in GSE co-ordinates).

Figure 2. A density plot of detected magnetopause crossings locations in GSM co-ordinates. Position ρ is defined as $\sqrt{{Y_{GSM}}^2 + {Z_{GSM}}^2}$ (see equation 3 for further details). The density of each bin is represented by the logarithmic color scale.

Figure 3. A histogram of the radial differences, as calculated in equation 1, between the detected crossing location and the *Petrinec and Russell* [1996] modeled magnetopause location. The three vertical dashed blue lines represent the lower interquartile, the median and the upper interquartile respectively.

Figure 4. A histogram, of the same form as Figure 3, for the *Shue et al.* [1998] model.

Figure 5. A histogram, of the same form as Figure 3, for the *Dmitriev and Suvorova* [2000] model.

Figure 6. A histogram, of the same form as Figure 3, for the *Lin et al.* [2010] model.

Figure 7. A comparison of the radial difference between the detected magnetopause location and the modeled locations for each of the three models, plotted for the four parameters (clock angle, B_z, P_d and spacecraft angle θ). The density of the bins is represented by the logarithmic color bar. The median radial difference for each row is denoted by the cross and the error bars represent the interquartile range of the row.

Figure 8. A comparison of the medians for the full population (blue) and the 20% sample (red), plotted again for the four parameters (clock angle, B_z, P_d and spacecraft angle θ). The solid lines indicate the median value for the row and the lightly shaded areas represent the interquartile range of each row.

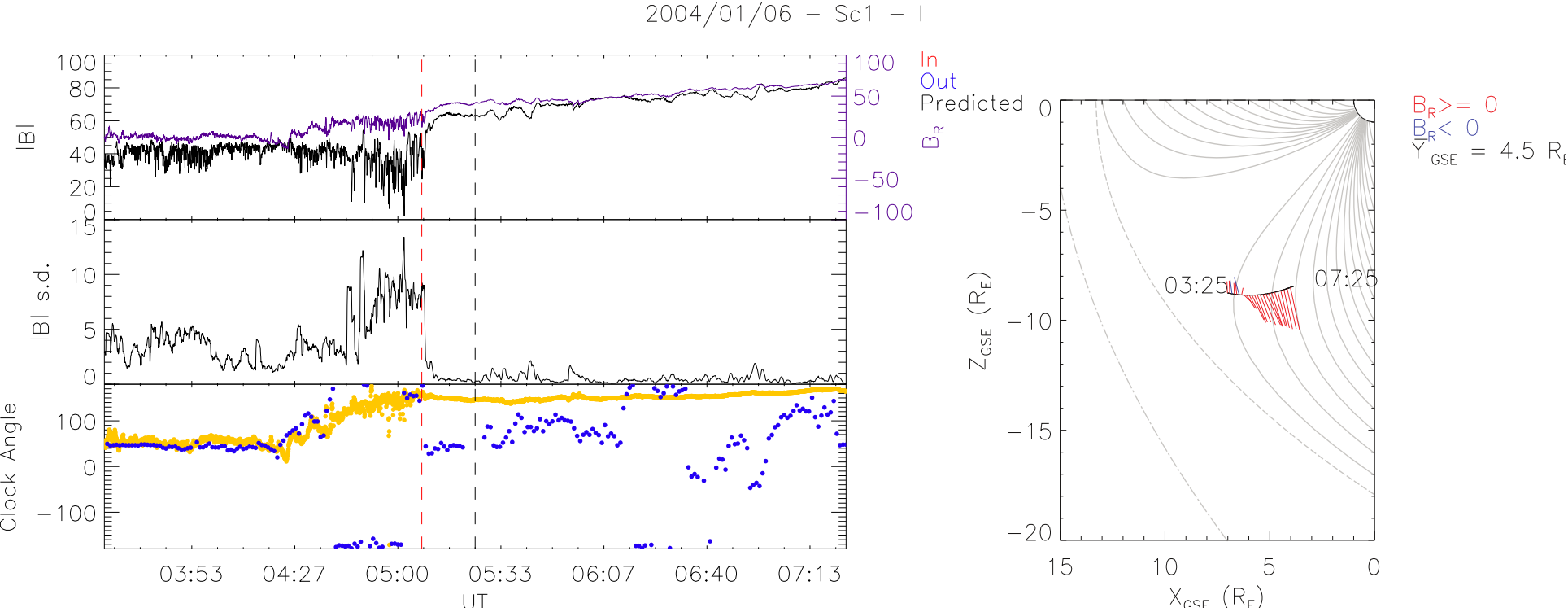
2004/01/06 – Sc1 – I
|B|
|B| s.d.
Clock Angle
In
Out
Predicted
B_R
100
80
60
40
20
0
15
10
5
0
100
0
−100
100
50
0
−50
−100
03:53
04:27
05:00
05:33
06:07
06:40
07:13
UT
B_R>= 0
B_R< 0
Y_{GSE} = 4.5 R_E
03:25
07:25
Z_{GSE} (R_E)
X_{GSE} (R_E)
0
−5
−10
−15
−20
15
10
5
0

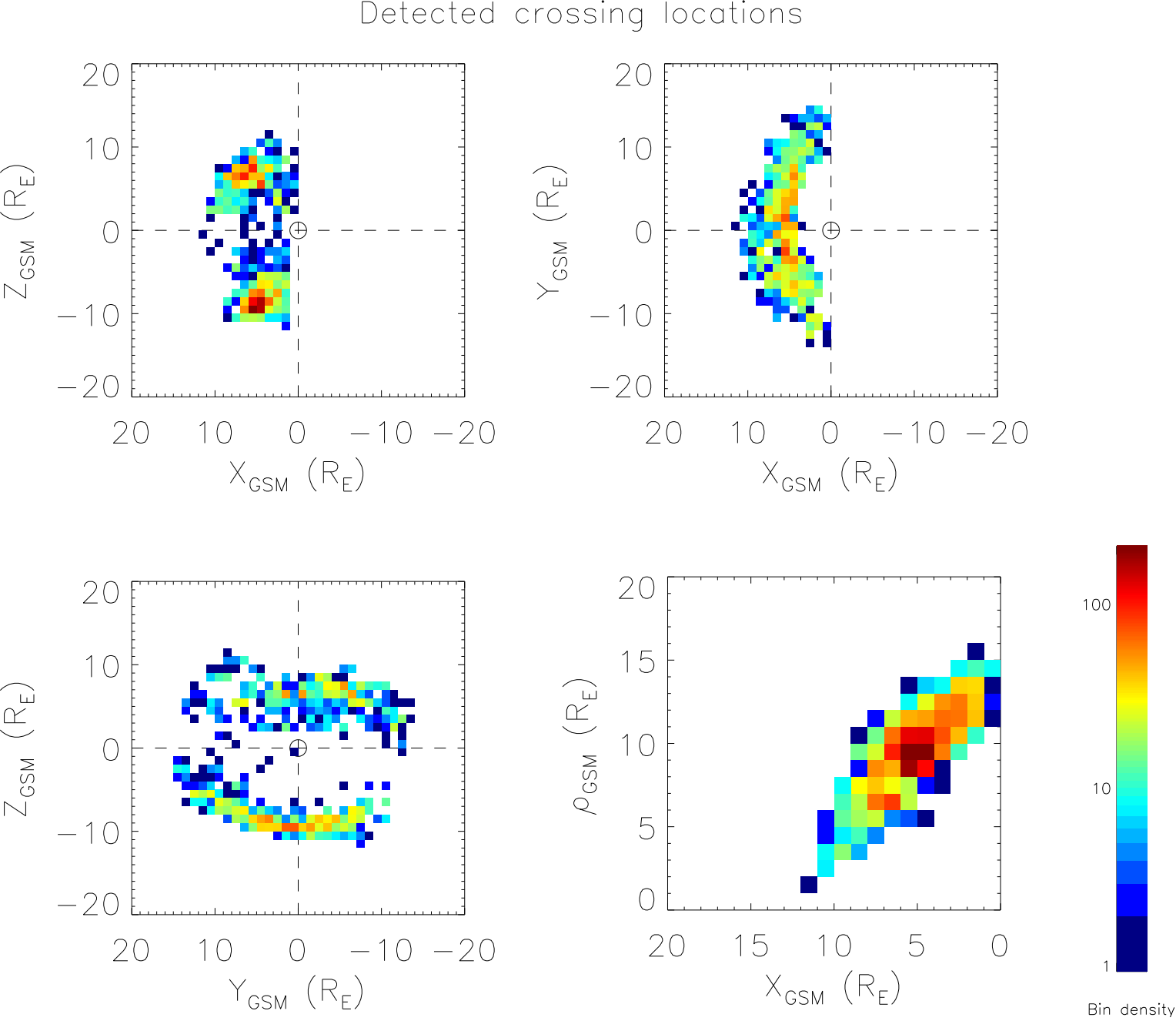
Detected crossing locations
Z_{GSM} (R_E)
X_{GSM} (R_E)
Y_{GSM} (R_E)
X_{GSM} (R_E)
Z_{GSM} (R_E)
Y_{GSM} (R_E)
ρ_{GSM} (R_E)
X_{GSM} (R_E)
Bin density
100
10
1

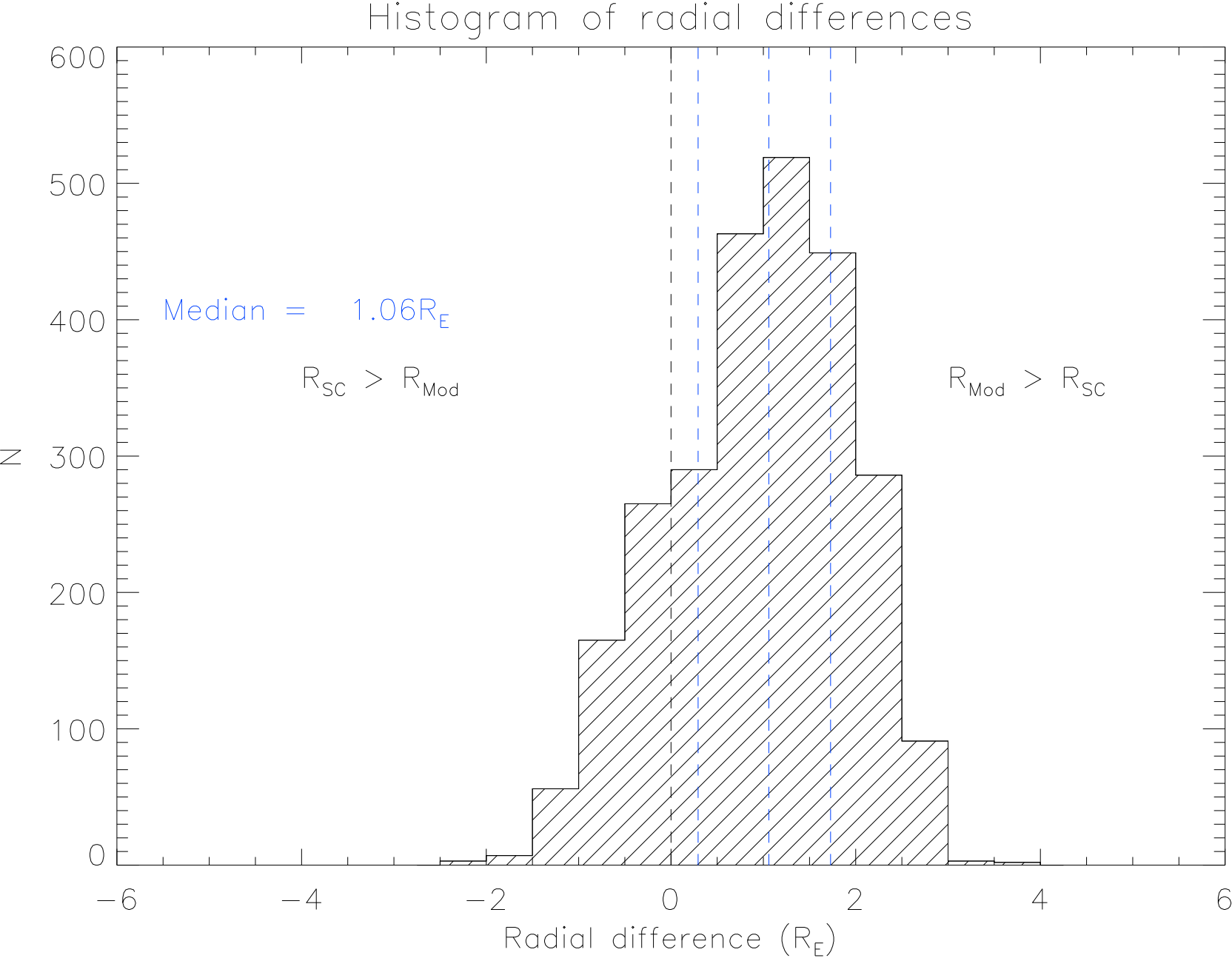
Histogram of radial differences
Median = 1.06R_E
R_SC > R_Mod
R_Mod > R_SC
N
Radial difference (R_E)
600
500
400
300
200
100
0
−6
−4
−2
0
2
4
6

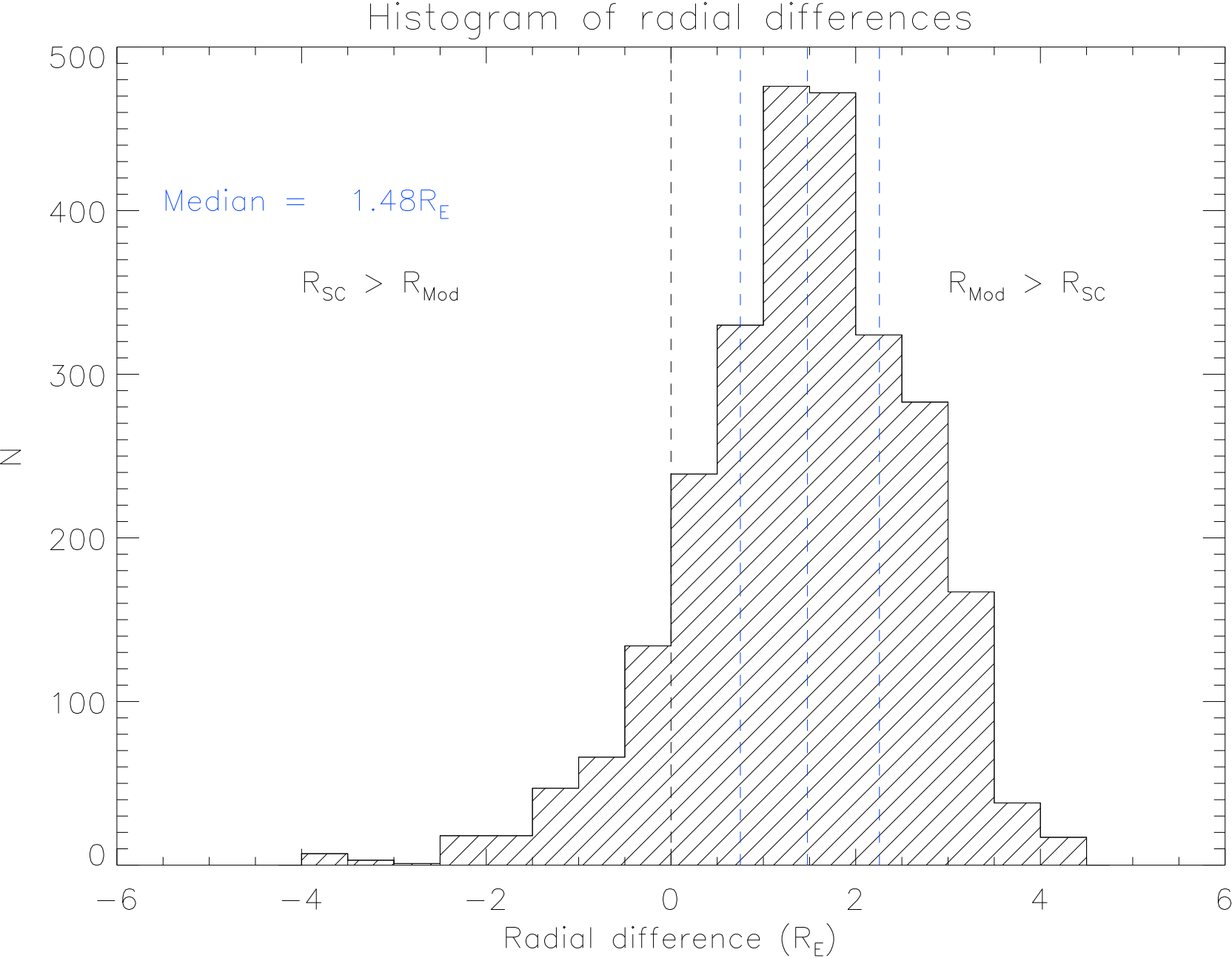
Histogram of radial differences
Median = 1.48R_E
R_SC > R_Mod
R_Mod > R_SC
N
Radial difference (R_E)
500
400
300
200
100
0
−6
−4
−2
0
2
4
6

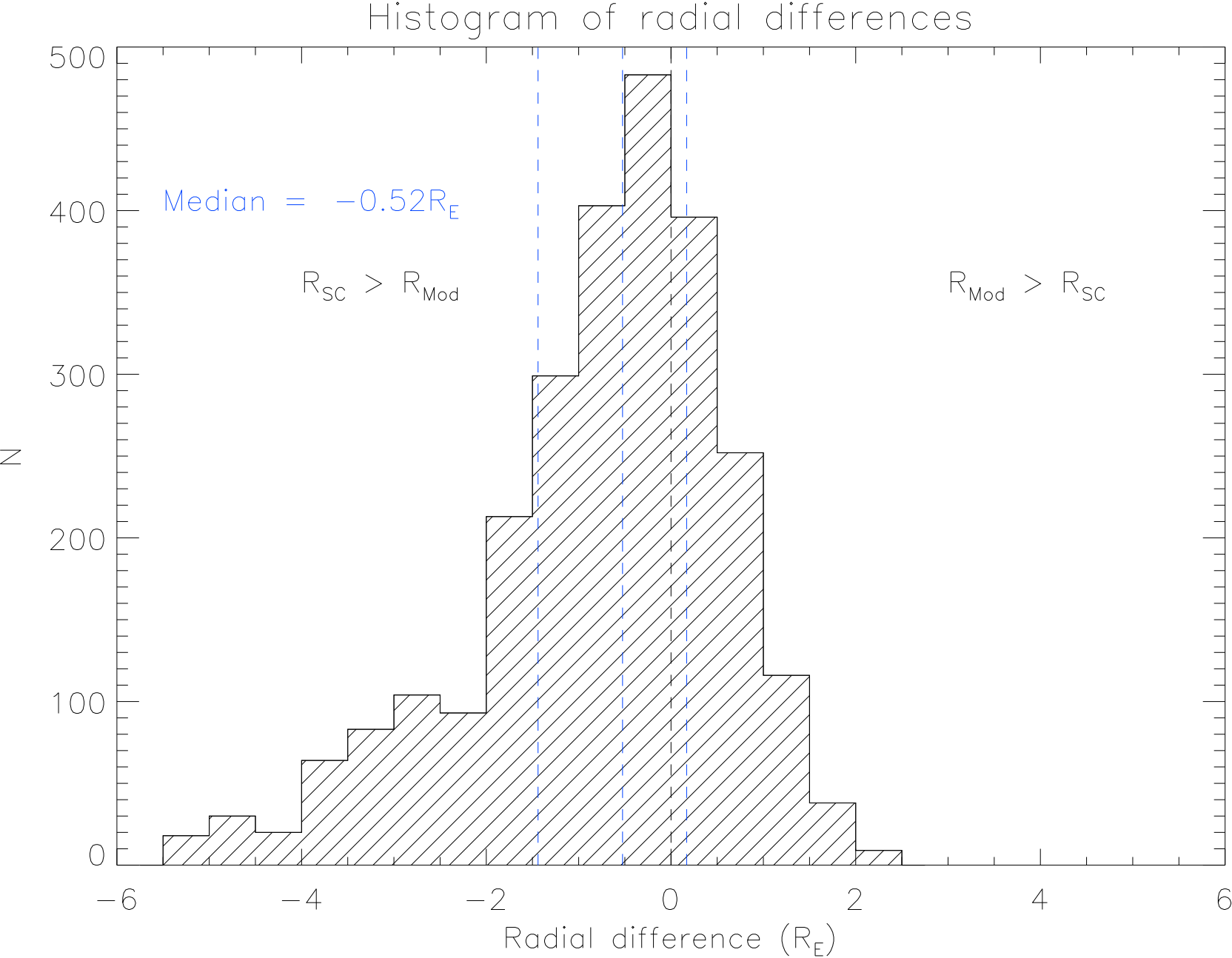
Histogram of radial differences
Median = −0.52R_E
R_SC > R_Mod
R_Mod > R_SC
N
Radial difference (R_E)
500
400
300
200
100
0
−6
−4
−2
0
2
4
6

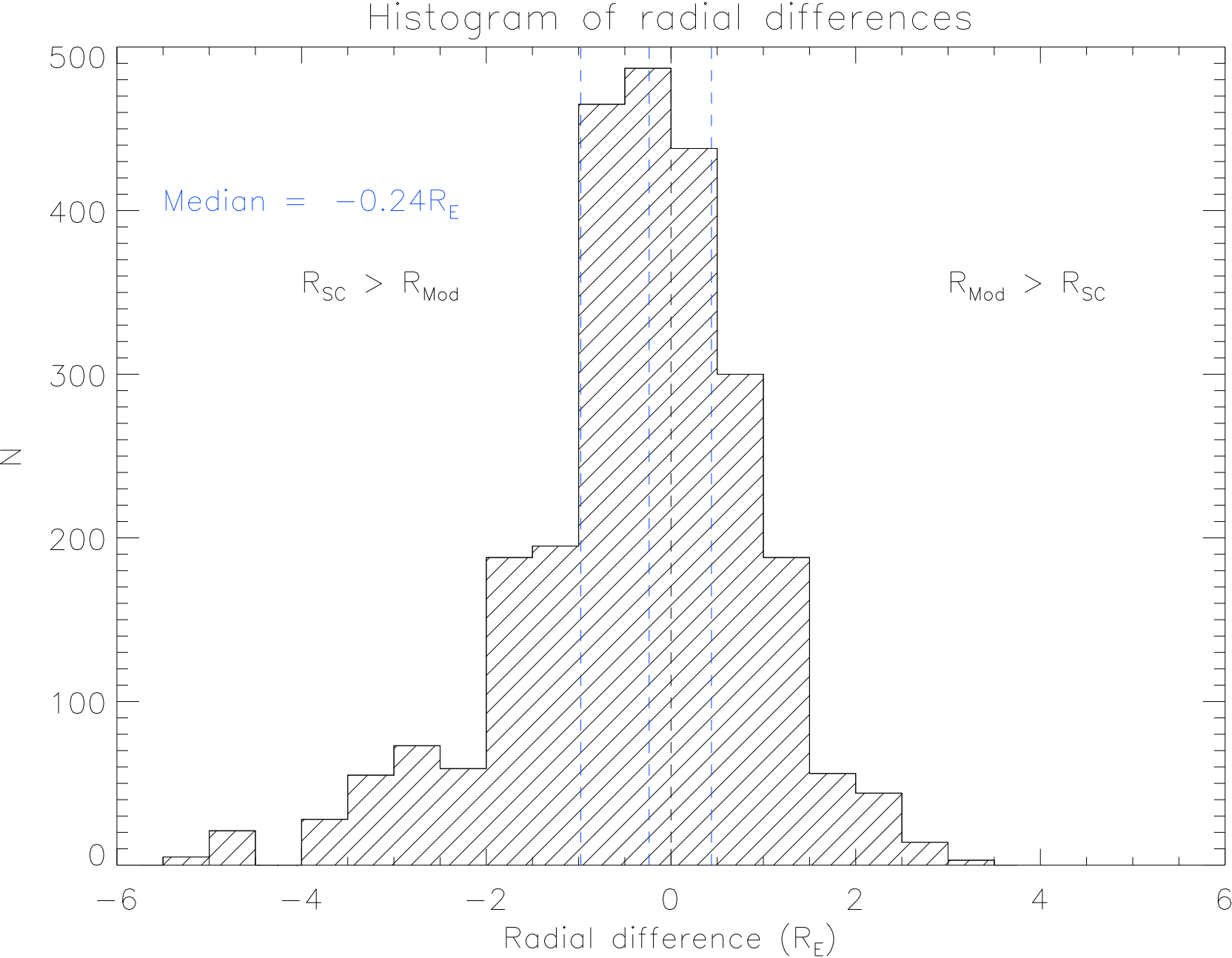
Histogram of radial differences
Median = −0.24R_E
R_SC > R_Mod
R_Mod > R_SC
N
Radial difference (R_E)
500
400
300
200
100
0
−6
−4
−2
0
2
4
6

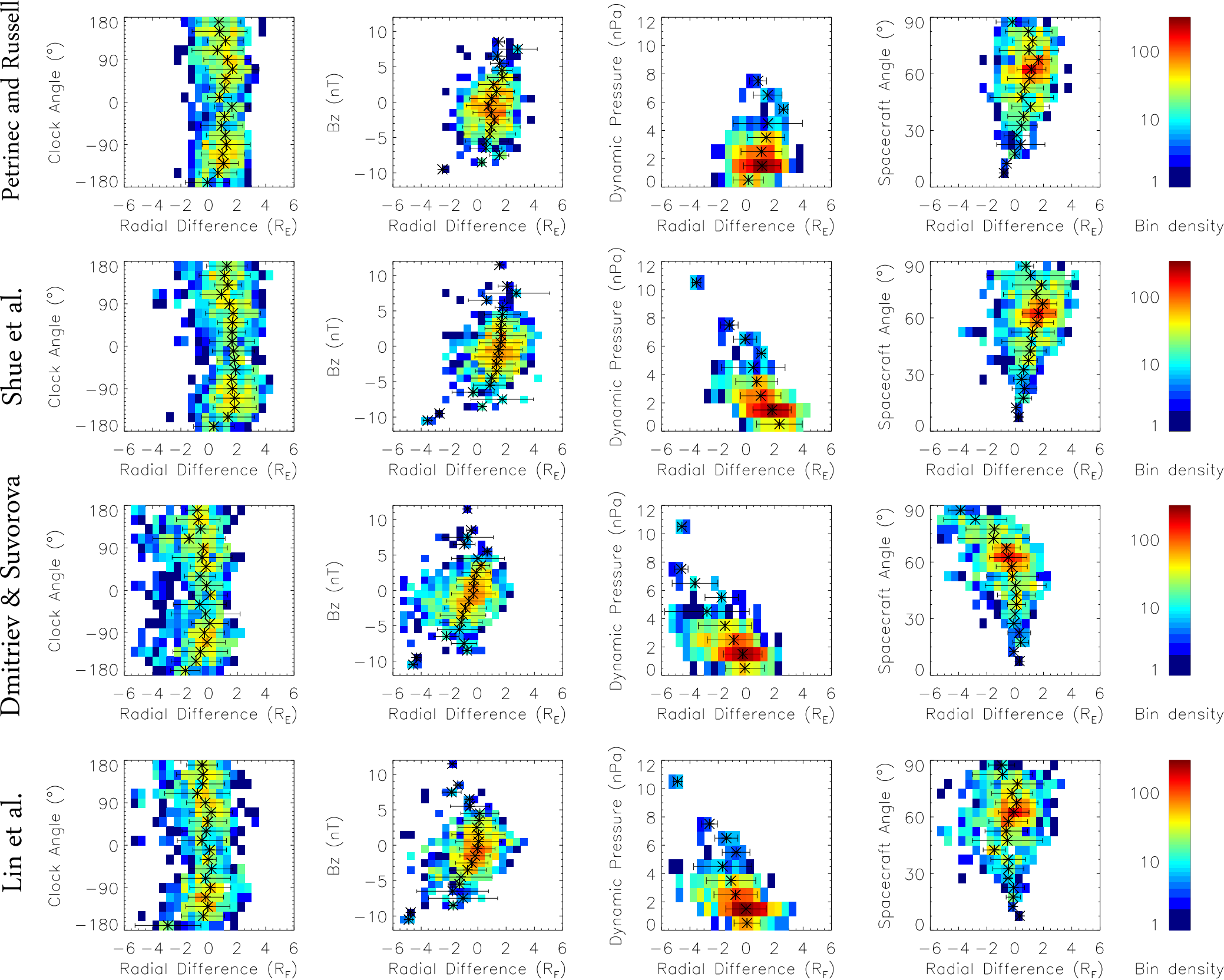
Petrinec and Russell
Shue et al.
Dmitriev & Suvorova
Lin et al.
Clock Angle (°)
Bz (nT)
Dynamic Pressure (nPa)
Spacecraft Angle (°)
Radial Difference (R_E)
Radial Difference (R_F)
Bin density

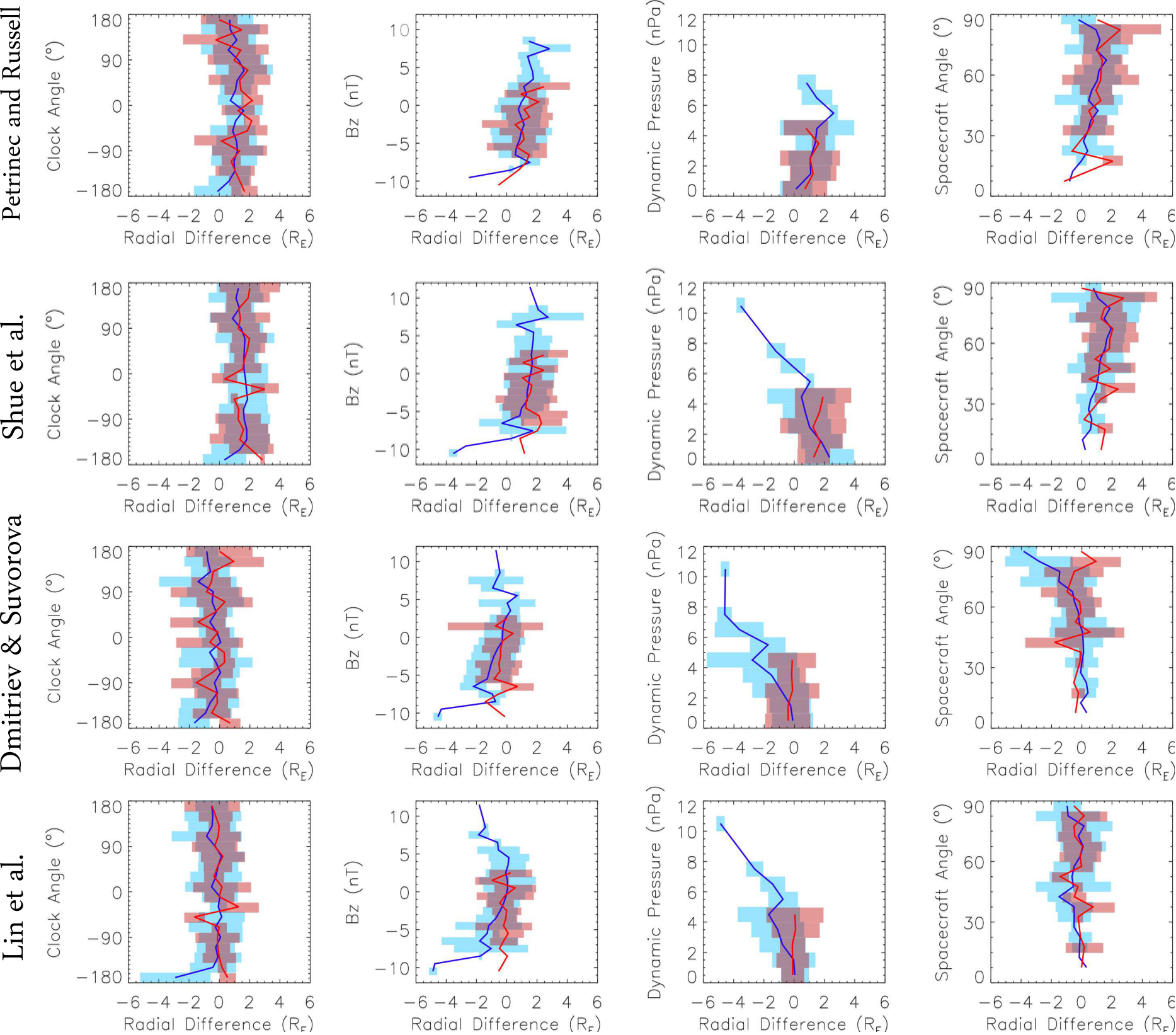
Petrinec and Russell
Shue et al.
Dmitriev & Suvorova
Lin et al.
Clock Angle (°)
Bz (nT)
Dynamic Pressure (nPa)
Spacecraft Angle (°)
Radial Difference (R_E)